Article
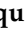
Susceptibility to Pitting Corrosion of Ti-CP2, Ti-6Al-2Sn-4Zr-2Mo, and Ti-6Al-4V Alloys for Aeronautical Applications

Jesus Jaquez-Muñoz [1], Citlalli Gaona-Tiburcio [1,*], Alejandro Lira-Martinez [1], Patricia Zambrano-Robledo [1], Erick Maldonado-Bandala [2], Oliver Samaniego-Gamez [1], Demetrio Nieves-Mendoza [2], Javier Olguin-Coca [3], Francisco Estupiñan-Lopez [1] and Facundo Almeraya-Calderon [1,*]

[1] Universidad Autonoma de Nuevo Leon, FIME-Centro de Investigación e Innovación en Ingeniería Aeronáutica (CIIIA), Av. Universidad s/n, Ciudad Universitaria, San Nicolás de los Garza 66455, Mexico; Jesus.jaquezmn@uanl.edu.mx (J.J.-M.); Manuel.lirama@uanl.edu.mx (A.L.-M.); patricia.zambranor@uanl.edu.mx (P.Z.-R.); pedro.samaniegogm@uanl.edu.mx (O.S.-G.); francisco.estupinanlop@uanl.edu.mx (F.E.-L.)
[2] Universidad Veracruzana, Facultad de Ingeniería Civil, Xalapa 91000, Mexico; erimaldonado@uv.mx (E.M.-B.); dnieves@uv.mx (D.N.-M.)
[3] Universidad Autónoma del Estado de Hidalgo, Área Académica de Ingeniería y Arquitectura, 42082 Carretera Pachuca-Tulancingo Km. 4.5., Pachuca de Soto 42082, Mexico; olguinc@uaeh.edu.mx
*   Correspondence: citlalli.gaonatbr@uanl.edu.mx (C.G.-T.); facundo.almerayacld@uanl.edu.mx (F.A.-C.)

Abstract: Titanium alloys are used in different industries like biomedical, aerospace, aeronautic, chemical, and naval. Those industries have high requirements with few damage tolerances. Therefore, they are necessary to use materials that present fatigue, mechanical, and corrosion resistance. Although Ti-alloys are material with high performance, they are exposed to corrosion in marine and industrial environments. This research shows the corrosion behavior of three titanium alloys, specifically Ti CP2, Ti-6Al-2Sn-4Zr-2Mo, and Ti-6Al-4V. Alloys were exposed on two electrolytes to a 3.5 wt % H_2SO_4 and NaCl solutions at room temperature using cyclic potentiodynamic polarization (CPP) and electrochemical noise (EN) according to ASTM G61 and ASTM G199 standards. CPP technique was employed to obtain electrochemical parameters as the passivation range (PR), corrosion type, passive layer persistence, corrosion potential (E_{corr}), and corrosion rate. EN was analyzed by power spectral density (PSD) in voltage. Results obtained revealed pseudopassivation in CPP and PSD exposed on NaCl for Ti-6Al-2Sn-4Zr-2Mo, indicating instability and corrosion rate lower. However, Ti-6Al-4V presented the highest corrosion rate in both electrolytes. Ti-6Al-2Sn-4Zr-2Mo revealed pseudopassivation in CPP and PSD in NaCl, indicating a passive layer unstable. However, the corrosion rate was lower in both solutions.

Keywords: corrosion; potentiodynamic polarization; PSD; titanium

1. Introduction

The titanium alloys offer attractive properties: high strength to weight ratio, high corrosion resistance, good formability, and biocompatibility, and thus are widely used in many applications. These alloys are used in aerospace, biomedical, chemical, and petrochemical industries [1–3]. The use of titanium alloys increased significantly in the 1980s, particularly in aircraft combat construction instead of civil aircraft. In the 1990s, for combat aircraft, titanium and aluminum alloy were at the same fraction of the structural weight in the 1990s. The aviation industry demands improvements in the characteristics of aircraft structural and functional material components based on scientific research conducted on new materials [2–4].

Titanium alloys can do identified into four types, Ti α, near to α, α + β, and metastable β. The microstructure depends on the β stabilizer (Mo, V, Cr, Ni, Fe, and Ta). α-Ti alloys

do denominate as commercially pure (CP) and highly pure titanium. The α Ti-alloys could have interstitial elements such as oxygen and nitrogen, titanium mechanical resistance but decreasing the ductility. For some cryogenic or high-temperature applications, α alloys add Al, Zr, or Sn as α stabilizers. If near α alloys combine α and $\alpha + \beta$ alloys properties, high-temperature resistance, and high mechanical resistance, they would have a 2% β stabilizer. Some new Ti-alloys add Si (0.1–0.5%) to improve their properties at high temperatures [5–9]. $\alpha + \beta$ alloys have more than one stabilizer α-phase (such as interstitial) and β-phase until 6%. The $\alpha + \beta$ phase is the most common, Ti-6Al-4V is the most used Ti-alloy globally, with almost 50% production. β-Ti alloys have a high percentage of β stabilizers and can present a martensitic microstructure. For this reason, the microstructure could be more complex [8–10].

The corrosion resistance of titanium alloys results from the formation of very stable, continuous, highly adherent, and protective oxide films on metal surfaces. Since titanium is highly reactive and has an extremely high affinity for oxygen, these beneficial surface oxide films spontaneously and instantly when new metal surfaces are exposed to air and moisture. Passivation of Ti alloy generates oxides coatings mainly composed of TiO_2 (rutile and anatase), Ti_2O_3, and TiO_5. depending on the environmental conditions, morphologically constituted by a two-layer structure [11,12].

Titanium alloys are subject to corrosion in specific environments. The primary forms of corrosion observed on these alloys include general corrosion, crevice corrosion, anodic pitting, hydrogen damage, and SCC. In any titanium application, its susceptibility to corrosion must be considered. Furthermore, the corrosion resistance of Ti alloys depends on their composition, microstructure, and surface treatment [5,13].

Sha et al. showed that when titanium does expose to sulfides, chlorides, and phosphate, titanium corrosion resistance decreases [8]. When Ti-alloys bring into contact with sulfides, a uniform attack occurs. The oxide layer creates on the metal surface deteriorates and dissolves, removing the corrosion protector. A Ti soluble ion goes to the electrolyte, $Ti \rightarrow Ti^{3+} + 3e^-$. The sulfuric acid chemical reaction is next $Ti + 2H_2SO_4 + 2e^- \rightarrow TiSO_4{}^{-2} + H_2$. A hydrogen reaction does present; this changes acid concentration and intensifies media aggressiveness [8–10,14–16]. For chloride, the mechanism is different, Cl^- provokes difficulties to TiO_2 layer growth, breaking the layer [17]. In some cases, Cl^- works as an interstitial element, being bigger than oxygen, and generates a diffusion process of Cl^- in the surface, creating instability in the passive layer [14,18].

Ti-6Al-4V presented fluctuation in the anodic reaction when exposed to artificial seawater, indicating instability [19]. Researchers adjudicate this behavior to impurities, roughness, and surface impurities in general [20]. In acid media, titanium oxide film could be broken, and metal surface exposed to the electrolyte directly, inducing an electrochemical reaction that increases corrosion rate [21]. Additionally, hydrogen diffusion could present when titanium is in H_2SO_4. The hydrogen diffusion can provoke embrittlement and make titanium susceptible to intergranular surface fracture [22]. Surface embrittlement induces a faster material dissolution and could increase the corrosion rate. The oxide layer is always not composed of TiO_2. Titanium dioxide does form by mitigation and adsorption of OH^- ions, localized in structural defects and the thinnest oxide layer zone [23]. The passive layer mechanism is determined by metal ions diffusion to the surface, transferring titanium and hydroxyl ions. If this oxide layer is creating, the layer will be stable [24–27].

However, Ti and its alloys' corrosion resistance links to oxide layer film formation. The oxygen reactive when Ti-alloys does expose to aqueous media [28,29]. Aggressiveness increase does attribute to pH change generated by a redox reaction. The hydrogen does dissociate and the pH electrolyte shifts. However, if temperature and pH are correctly combinate, a stable oxide layer could be created on the titanium surface [30,31]. Ti-alloys have been showing higher corrosion rates in alkaline and neutral media than in acidic media. The presence of OH^- and Cl^- ions accelerate the corrosion rate because those ions can destroy passive films.

Meanwhile, acid films based on H_2SO_4 generate a better layer [32], sulfate ions suppress chlorines activation, retarding the corrosion process [33,34]. As a passive film does form, when titanium has been exposed in a media for a long time, chloride ions' oxide layer increase and diffusion occurs [34].

When Ti-alloys are exposed in NaCl it could provoke pitting and challenging to generate a stable oxide layer. Although some researchers have been demonstrated that corrosion density and pitting potential decrease when Cl^- concentration increases. Additionally, Cl^- heterogeneous distribution is deposited in localized surface zones, and the passive film will break it [33–35]. Others factor that can promote localized process is microstructure, grain refinement, and surface roughness [28,36]. The oxide layer could be different depending on the Ti phase. It is usually the case that the layer is denser in α than β, this is because, in α, the oxide layer creates a significant part of the TiO_2 and β for vanadium oxide (Ti-6Al-4V) [28–33].

Studies about pitting and breakdown of the passive layer have been developed and discussion is about Cl^- behavior. Almost all researchers agree with an adsorption process, but penetration is unclear [34–36]. Some researchers found a concentration of Cl- ions in the metal-layer interface, indicating a penetration through the oxide layer, hindering material passivation by oxide vacancy [37–39]. Additionally, phase discontinuity provokes the heterogeneous passive layer and ions susceptibility [40,41].

Different conventional electrochemical techniques such as linear polarization resistance (LPR), potentiodynamic polarization (PP), and electrochemical impedance spectroscopy (EIS) have been implemented to determine the corrosion and kinetic mechanisms of the reactions. In CPP curves, analysis of the cathodic and anodic reactions and the hysteresis curve can yield information about the corrosion mechanism in the system and the corrosion rates. The use of the electrochemical noise (EN) technique for investigation and monitoring of corrosion has allowed many advances that are interesting for corrosion science interesting advances in advances in recent years. A special advantage of electrochemical noise measurements is the possibility to detect and analyze the early stages of localized corrosion [42–46].

A cathodic reaction explains the process of hydrogen evolution and an anodic reaction explains the corrosion process and passivation. When current demand stops, a passive layer was developed, the potential range since current demand stopped until it is reactivated will be known as the passive range. Potentiodynamic polarization curves are a helpful tool to find the corrosion type present based on hysteresis, if it is positive (right) that can be considered localized corrosion and if it is negative (left) it corresponds to uniform corrosion. Additionally, hysteresis can provide more information about passive behavior. If hysteresis is great, it means difficult to restore passivity [45–52].

EN analyzes reactions in a metal surface by different methods, recommends applying a filter to separate random and stationery components from the DC signal, and obtained the corrosion system signal [53,54].

$$x\,(t) = m_t + s_t + Y_t \tag{1}$$

Being x (t) is the EN signal, m_t is the DC component, s_t is random, and Y_t for stationary components. To filter this signal it is necessary to apply a polynomial, defined by Equation (2), where the noise signal (x_n) is filtered by a grade "n" polynomial (p_o) at the n-th term (a_i) to obtain a signal without trend (Y_n) [22,55].

$$Y_n = x_n - \Sigma^{po}_{i=0} a_i n^i \tag{2}$$

The power spectral density (PSD) analysis must transform from time-domain to frequency-domain signal applying FFT, shown in Equations (3) and (4) [55].

$$R_{xx}\,(m) = (1/N) \Sigma_{n=0}^{N-m-1} \tag{3}$$

$$\Psi_x(k) = \frac{\gamma \cdot t_m}{N} \cdot \sum_{n=1}^{N} (x_n - \overline{x}_n) \cdot e^{\frac{-2\pi k n^2}{N}} \tag{4}$$

With PSD voltage it is possible to evaluate passive layer behavior, whether it is homogenous or not, and in some cases could provide mechanistic information about the corrosion process. The values of corrosion type are shown in Table 1 [56–58].

Table 1. Chemical composition of the used titanium alloys (wt %).

Alloys	Elements		
	Ti CP2	**Ti-6Al-2Sn-4Zr-2Mo**	**Ti-6Al-4V**
Fe	0.038 ± 0.005	–	0.21 ± 0.01
Al	–	6.75 ± 0.20	7.14 ± 0.37
V	–	–	4.03 ± 0.08
Zr	–	4.18 ± 0.01	–
Mo	–	1.99 ± 0.008	–
Sn	–	2.08 ± 0.01	–
Ti	99.94 ± 0.005	84.65 ± 0.19	87.71 ± 0.36

The aim was studying the susceptibility of pitting corrosion on three Ti-alloys, Ti CP2, Ti-6Al-2Sn-4Zr-2Mo, and Ti-6Al-4V, immersed at 3.5 wt % in H_2SO_4 and NaCl solutions at room temperature by cyclic potentiodynamic polarization (CPP) and power spectral density (PSD) obtained from EN voltage series. The Ti-alloys could find potential applications in the aeronautical industry, like turbine blades and aircraft landing gear. Components made of superalloys are exposed to various chemical agents. These Ti-alloys are susceptible to low temperature pitting corrosion when aircraft are in marine and industrial environments.

2. Materials and Methods

2.1. Material

The alloys used for this research were Ti-6Al-2Sn-4Zr-2Mo, Ti-6Al-4V, and Ti CP2 used in the received condition. The chemical composition was obtained by X-ray fluorescence (XRF) (Olympus DELTA XRF, Richmond, Texas, USA). Table 1 shows the chemical composition of each Ti-alloy.

Titanium alloys selected in this research have different metallurgical characteristics. Titanium Grade 2 CP (α-type Ti alloys) is generally known as the commercially pure titanium (unalloyed). Due to its varied usability and broader availability, it has been used in many applications. The Ti6Al4V alloy (one of the α + β type of Ti alloys), designated as ASTM B265 Grade 5, is the most commonly used because it has excellent mechanical properties and is considered the military grade titanium. Ti-6Al-2Sn-4Zr-2Mo, also known as Ti 6-2-4-2, is a near alpha titanium alloy known for its high strength and excellent corrosion resistance. It is often used in the aerospace industry to create high-temperature jet engines and the automotive industry to create high-performance automotive valves.

2.2. Microstructural Characterization

Specimens were polished using metallographic techniques according to ASTM E3 [59]. The material was sequentially polished using different SiC grit papers with 400, 600, and 800 grades, followed by cleaned ultrasonically in ethanol (C_2H_5OH) and rinsed with distilled water for 10 min. The etching of polish samples does elaborate with a Kroll solution composed of 3 mL HF, 5 mL HNO_3, and 100 mL water, based on ASTM E 407 [60].

The microstructural analysis was carried by optical microscopy (OM, Olympus, Hamburg, Germany) and scanning electron microscopy (SEM, JEOL-JSM-5610LV, Tokyo, Japan) for identifying the microstructure of samples a magnification of $500\times$ and $1000\times$ oper-

ating at 20 kV, WD = 14 mm. The chemical composition of these alloys was obtained by energy-dispersive X-ray spectroscopy (EDS, JEOL-JSM-5610LV, Tokyo, Japan).

2.3. Electrochemical Techniques

The electrochemical techniques of cyclic potentiodynamic polarization (CPP) and electrochemical noise (EN) were used to determine the corrosion kinetics of titanium alloys. The CPP was recorded at a sweep rate of 0.06 V/min, a potential scan range was applied between −1.0 and 1.2 V vs. SCE from the corrosion potential (Ecorr), using a complete polarization cycle, according to ASTM G5-14e1 [61] and ASTM G61 standards [59]. Corrosion experiments were performed by immersion of the titanium alloy specimens, with an exposed surface area of 1.0 cm^2, in 3.5 wt % NaCl and H$_2$SO$_4$ solutions, this latter to simulate an acid rain environment at room temperature. A conventional three-electrode cell configuration was used for electrochemical studies, which consisted of a working electrode (titanium alloys). A saturated calomel electrode (SCE) and a platinum mesh were used as reference and counter electrodes [23].

In CPP curves, analysis of the cathodic and anodic reactions and the hysteresis curve can yield information about the mechanism of corrosion in the system and the corrosion rates. Tafel extrapolation of potentiodynamic polarization curves is employed to determine the corrosion current density, i_{corr} (mA·cm^{-2}), and corrosion rate [42–45,52,61,62].

The corrosion kinetic behavior using potentiodynamic polarization can be observed through cathodic and anodic reactions in polarization curves. The corrosion rate in terms of penetration (mm/s) is one of the main parameters obtained by potentiodynamic polarization curves, according to Faraday's law (Equation (5)) [46–49].

$$Corrosion\ rate = \frac{K \cdot i_{corr}}{\rho \cdot E.W} \tag{5}$$

where *E.W* = equivalent weight, i_{corr} = current density in μA/cm^2, *K* is a corrosion rate constant and ρ = density in g/cm^3.

According to the ASTM G199-09 standard [63], EN measurements were carried out, allowing the noise resistance (Rn) and corrosion rate evaluation to determine in a corrosive medium. For each experiment, two nominally identical specimens were used as the working electrodes (WE1 and WE2) and a saturated calomel electrode as the reference electrode (RE). Measured electrochemical current noise (ECN) was with galvanic coupling current between two identical working electrodes; simultaneously, electrochemical potential noise (EPN) was measured linking one of the working electrodes and reference electrodes. Monitored the current and potential electrochemical noise was concerning time for each electrode–electrolyte combination. For each set of EN measurements, obtained 4096 data points were with a scanning rate of 1 data/s EN data was processed with a program made in MATLAB 2018a software ((Math Works, Natick, MA, USA accessed on 15/05/2021). It removes the trends with a polynomial grade 9 and fast Fourier transformed (FFT) with a Hann windowing [5,56]. The electrochemical measurements were recorded simultaneously using a Gill-AC potentiostat/galvanostat/ZRA (zero resistance ammeter) from ACM Instruments. All the electrochemical tests were performed in triplicate.

3. Results

3.1. OM—SEM Microstructural Analysis

An OM and SEM analyzed the microstructures of the samples in initial conditions. Figure 1a shows a matrix of α phase microstructure for Ti CP2, with large grain size. Figure 1b shows the Ti-6Al-2Sn-4Zr-2Mo microstructure. Ti-6Al-2Sn-4Zr-2Mo has α-phase grains, with a light-appreciable deformation and angular shapes located at triple point unions corresponding to the β phase. Figure 1c shows the Ti-6Al-4V microstructure; this one is fine and equiaxial. α and β phases are marked with yellow arrows. This phase presents spherical shapes and α phases. The vanadium presence in Ti-6Al-4V increases the distribution of the β phase. The SEM analysis corroborates results and shows the porosity

with diameters of 1–2 μm. Porosity is presented in 1.68%, 2.87%, and 1.75% for Ti CP2, Ti-6Al-2Sn-4Zr-2Mo, and Ti-6Al-4V, respectively.
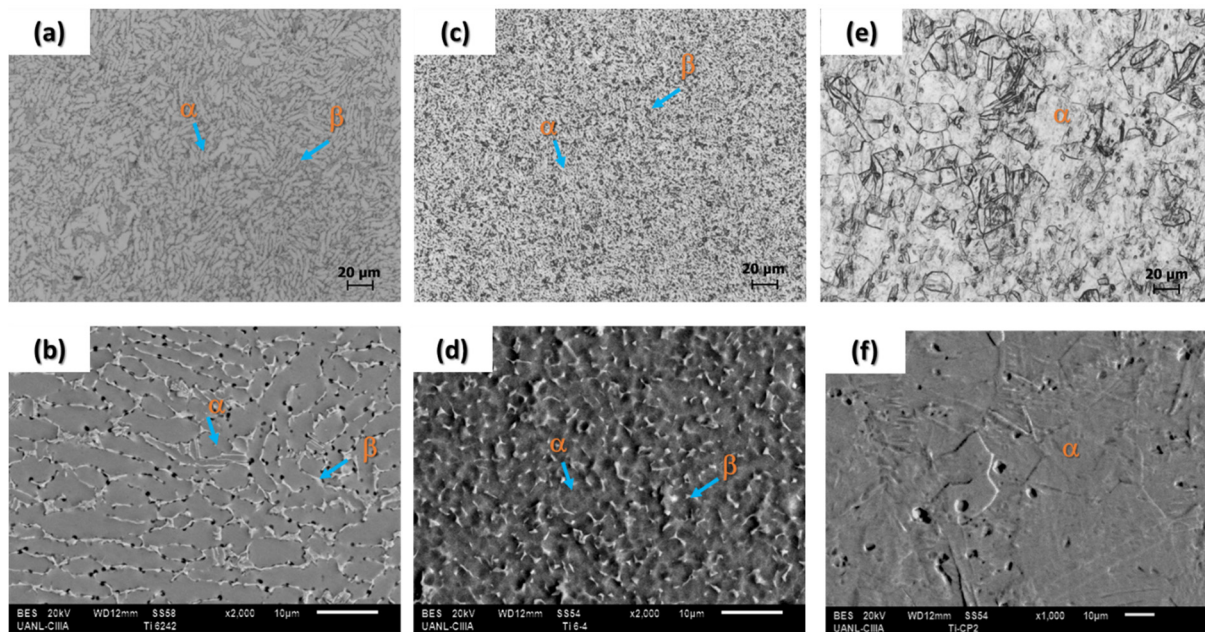
Figure 1. OM and SEM micrograph of titanium alloys (initial conditions): (**a**,**b**) Ti-6Al-2Sn-4Zr-2Mo, (**c**,**d**) Ti-6Al-4V, and (**e**,**f**) Ti CP2.

3.2. Electrochemical Test

3.2.1. Cyclic Potentiodynamic Polarization (CPP)

The cyclic potentiodynamic polarization curves are shown in Figures 2 and 3.

Figure 2 corresponds to titanium alloys in a 3.5 wt % NaCl solution. The anodic and cathodic reactions present a mixed activation control. Ti-6Al-2Sn-4Zr-2Mo shows a pseudopassivation behavior related to an unstable passive layer on the metal surface in the anodic region. Meanwhile, Ti CP2 and Ti-6Al-4V show passivation in a range of 1.025 and 1.104 V (see Table 2). Ti CP2 had a more active potential of −0.490 V, while Ti-6Al-4V had the noblest potential of −0.394 V. In the NaCl solution, Ti-6Al-4V shows the high E_{corr} and the higher passivation range, Ti-6Al-4V (1.104 V). Additionally, it presents a lower E_{a-c} (−0.230 V) in comparison with 0.286 V of Ti CP2, indicating that the passive layer is steadier Ti-6Al-4V than Ti CP2. Ti-6Al-2Sn-4Zr-2Mo showed pseudopassivation and not passivation and presented 3.07×10^{-4} mA·cm^{-2} i_{corr}. Low corrosion rate values were obtained, which is presented in Table 3 with 2.67×10^{-4} mm/y. Ti-6Al-4V showed the highest corrosion rate in NaCl with 5.9×10^{-4} mm/y, meaning that potential nobility and passivation range were not strictly related to a low corrosion rate. The reverse loop of Ti-6Al-2Sn-4Zr-2Mo and Ti-6Al-4V presents anodic reactions, so the passive layer became unstable when the potential was in reverse. In all cases, the results show a negative hysteresis, and this behavior indicates a uniform corrosion process. Additionally, the current demand presented at E_{a-c} was lower in order than in E_{corr}, suggesting that the oxide layer on metal surfaces reduces current demand. The adjustments to use the Tafel extrapolation in the potentiodynamic polarization curves (Figures 2 and 3) were made in an interval of ± 50 mV/OCP, using the software from ACM instruments.
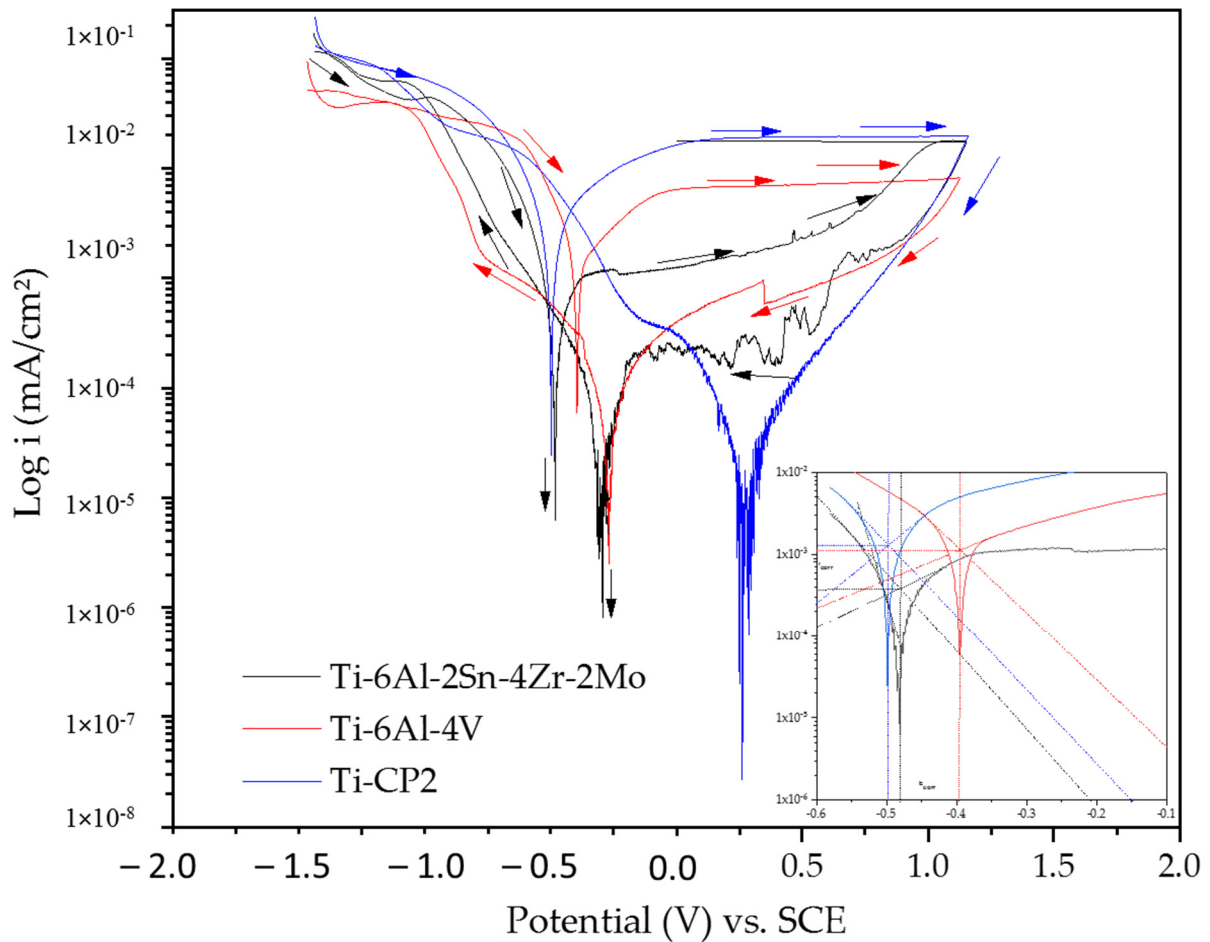
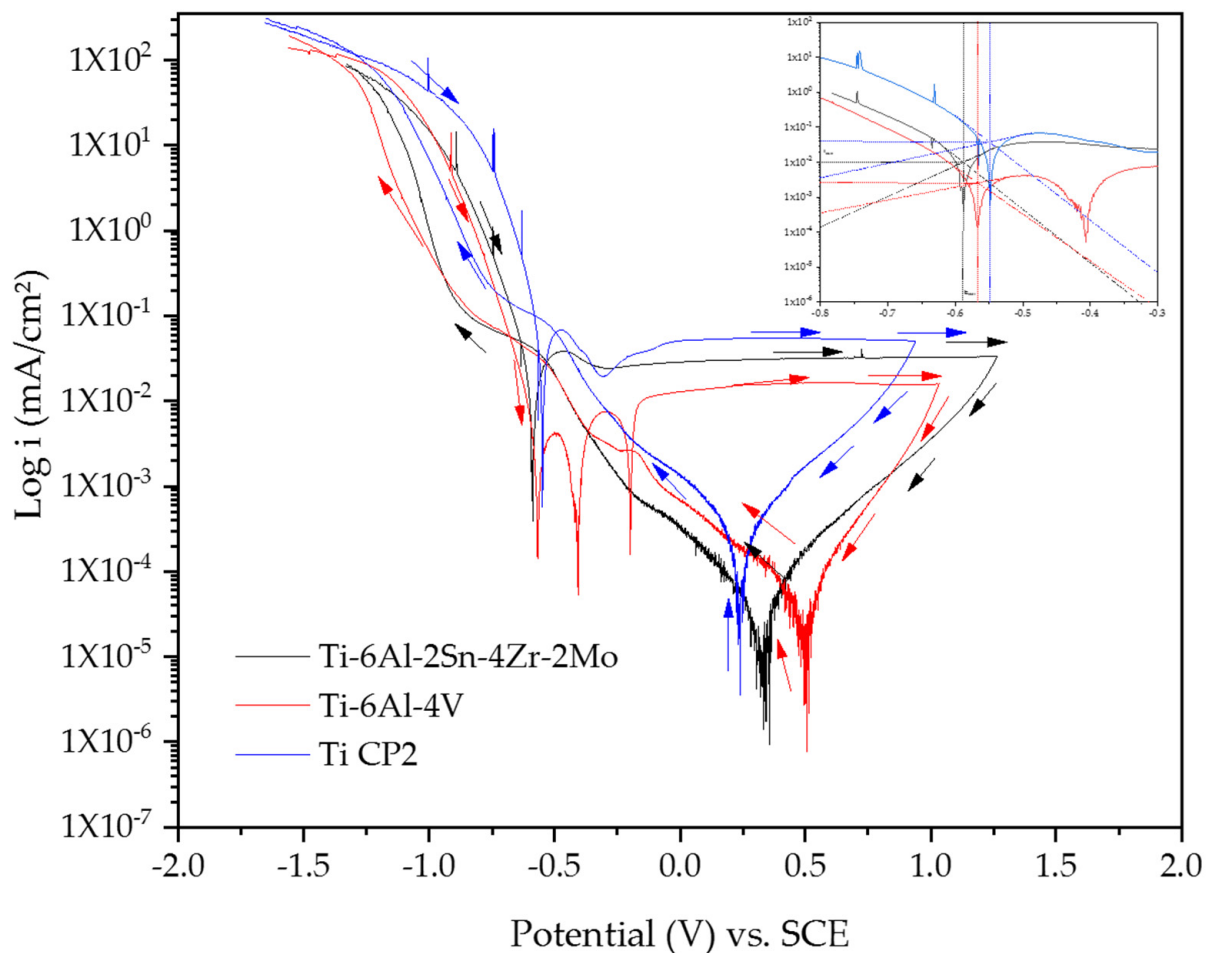**Figure 2.** Cyclic potentiodynamic polarization curves of titanium alloys exposed in a 3.5 wt % NaCl solution.

Table 2. Cyclic potentiodynamic polarization parameters in titanium alloys, in 3.5 wt % NaCl and H_2SO_4 solutions.

Alloys	E_{corr} (V)	i_{corr} (mA/cm^2)	$E_{a\text{-}c}$ (V)	Active-Passive Trans (V)	Hysteresis	Range Passive (V)	C.R. (mm/y)
			NaCl				
Ti-6Al-2Sn-4Zr-2Mo	−0.484	3.07×10^{-4}	N/A	–	Negative	–	2.67×10^{-4}
Ti-6Al-4V	−0.394	13.1×10^{-3}	0.230	–	Negative	1.104	5.90×10^{-4}
Ti CP2	−0.490	10.3×10^{-3}	0.286	–	Negative	1.025	5.26×10^{-4}
			H_2SO_4				
Ti-6Al-2Sn-4Zr-2Mo	−0.589	10.0×10^{-3}	−0.297	−0.477	Negative	1.739	1.06×10^{-2}
Ti-6Al-4V	−0.561	1.45×10^{-3}	−0.269	–	Negative	0.929	3.74×10^{-1}
Ti CP2	−0.547	2.91×10^{-3}	0.232	−0.479	Negative	1.156	1.20×10^{-1}

Table 3. Intervals of β values of PSD to determine corrosion type.

| Corrosion Type	dB(V)·Decade^{-1}		dB(A)·Decade^{-1}	
	Minimum	Maximum	Minimum	Maximum
Uniform	0	−7	0	−7
Pitting	−20	−25	−7	−14
Passive	−15	−25	−1	1

Figure 3 shows cyclic potentiodynamic polarization curves of Ti-alloys immersed in 3.5 wt % H_2SO_4 solution. Results showed that Ti-alloys have anodic and cathodic reactions that present a mixed activation control. The corrosion potential is similar to those obtained in NaCl, having the following values: Ti CP2 (-0.547 V), Ti-6Al-4V (-0.561 V), and Ti-6Al-2Sn-4Zr-2Mo (-0.589 V). Ti-alloys in H_2SO_4 solution have the potentials more active, as was Ti-6Al-2Sn-4Zr-2Mo with the highest passivation range (1.739 V). The passive range of Ti CP2 is 1.156 V representing the noblest potential and a negative passivation slope associated with an increase in passive layer efficiency that decreases current demand on the titanium surface. Ti 6Al-2Sn-4Zr2Mo and Ti CP2 presented an active–passive transition with nobler potential than E_{corr}. The active–passive transition occurs when there are susceptible to passivation and passivation film restoration, pitting, and localized corrosion are not typical with this behavior. E_{a-c} confirms that Ti CP2 had a more stable passive layer because the potential was nearest to E_{corr} than in other alloys. Ti-6Al-4V exhibited three E_{corr}; this behavior is known as a cathodic loop, associated with a reduction of passive layer by OH^- reactions. The OH^- reactions reduce the passive range of alloy and increase i_{corr} (4×10^{-2} mA·cm^{-2}). In the last sample, the passive range is related to the corrosion rate, the passive range was lower than in other alloys, and the corrosion rate was higher (with 3.47×10^{-1} mm/y). Besides, the Ti-6Al-2Sn-4Zr-2Mo passive range was associated with a corrosion rate of 10.06×10^{-2} mm/y, being lower. In H_2SO_4, the passive layer was directly related to corrosion rates. Suppose the passive layer persists at different potentials values, the corrosion rate decreased. All samples presented uniform corrosion.

Figure 3. Cyclic potentiodynamic polarization curves of titanium alloys exposed in a 3.5 wt % H_2SO_4 solution.

Figure 4a,b shows the corrosion rate behavior in NaCl and H₂SO₄ solutions. In both solutions, Ti-6Al-2Sn-4Zr-2Mo presented a lower corrosion rate. Meanwhile, the higher corrosion rate was for Ti-6Al-4V. Corrosion rate values were higher for H₂SO₄ solution with values of 10^{-2} and 10^{-1} to 10^{-4} mm/y to NaCl solution.
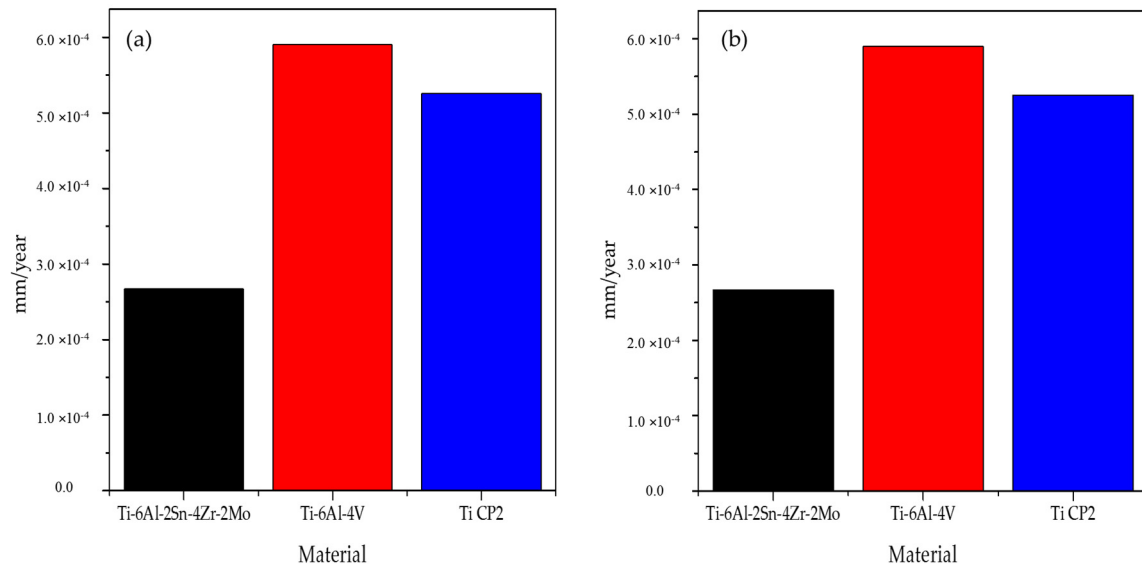
Figure 4. Corrosion rates in (**a**) NaCl and (**b**) H₂SO₄ Solutions.

3.2.2. Power Spectral Density Analysis (PSD)

For PSD analysis is necessary to transform to frequency-domain from time-domain applying an FFT (with a polynomial filter applied), spectral density do calculate with Equations (6) and (7) [64].

$$R_{xx}(m) = \frac{1}{N} \sum_{n=0}^{N-m-1} x(n) \cdot x(n+m), \quad \text{when values are from } 0 < m < N \tag{6}$$

$$\Psi_x(k) = \frac{\gamma \cdot t_m}{N} \cdot \sum_{n=1}^{N} (x_n - \overline{x}_n) \cdot e^{\frac{-2\pi k n^2}{N}} \tag{7}$$

The interpretation of PSD is based on the slope. The slope could be helpful to determine the type of corrosion [35]. It is defined by β_x and is represented by Equation (8):

$$log\Psi_x = -\beta_x \log f \tag{8}$$

PSD voltage shows potential (dBe) vs. frequency (Hz). In the NaCl solution, Figure 5a presents three alloys comparison. In Figure 4b, Ti-6Al-2Sn-4Zr-2Mo shows fluctuations in power values at high frequencies, indicating an unstable passive layer developed. Besides, a slope value of -20 dBe (see Table 3) marked with a green line was related to a passive system. In Figure 5c,d, the behavior was more stable, but the slope for Ti-6Al-4V and Ti CP2 was -11 and -11; those values are not in the parameters. However, the stable behavior in potential was associated with a passive or uniform corrosion process.

Figure 6a shows the Ti-alloys comparison PSD in the H₂SO₄ solution. For Ti-6Al-2Sn-4Zr-2Mo, Figure 5b shows a stable slope, Table 3 indicates that the slope value was -7, related to uniform corrosion. On the other hand, Ti-6Al-4V and Ti CP2 revealed that values were not within type corrosion slope values, -13 and -8 dB (A), respectively, but they could associate with a passive or uniform corrosion process like NaCl solution (see Table 4).
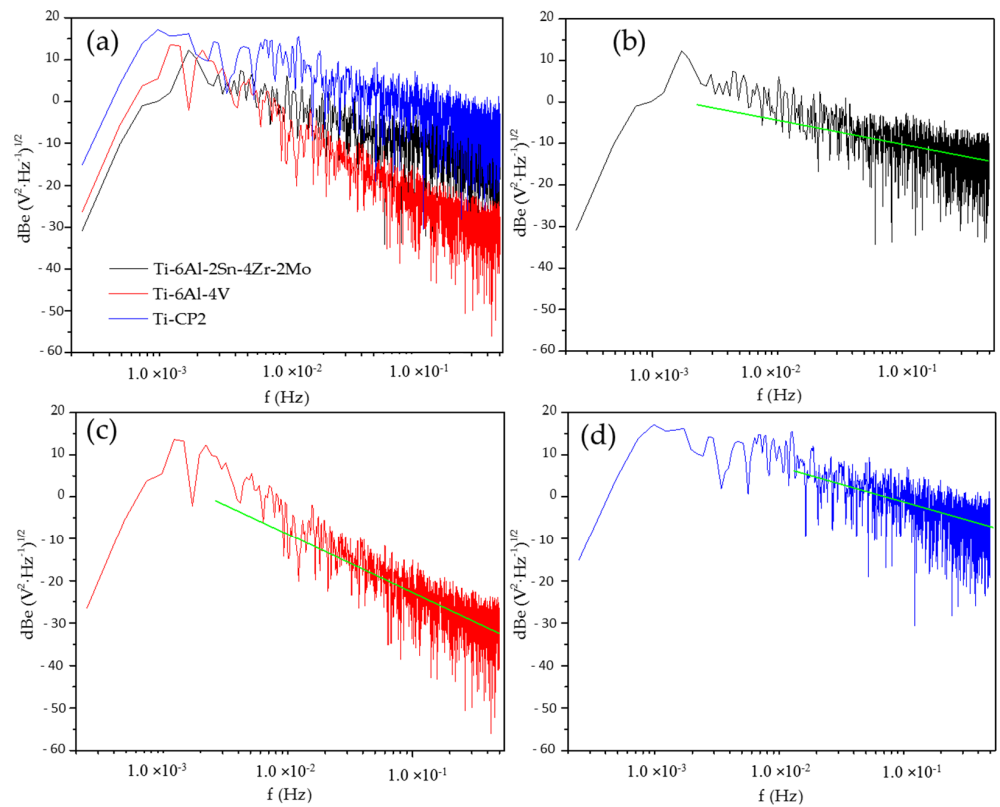
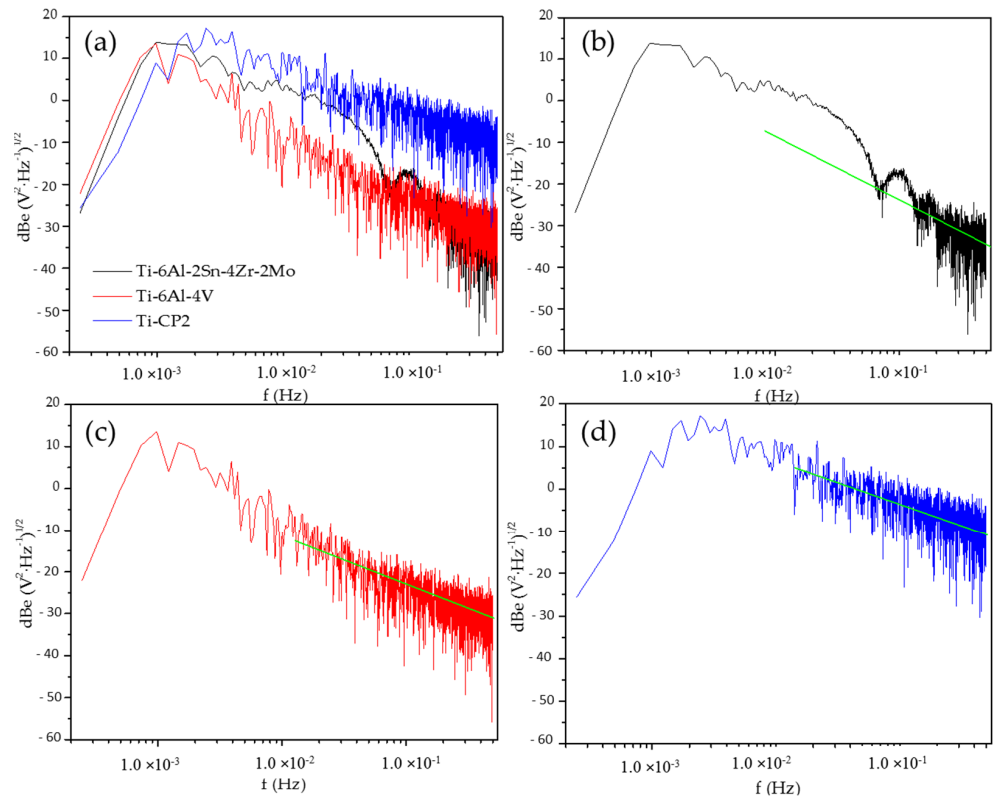**Figure 5.** PSD voltage in NaCl (**a**) all samples, (**b**) Ti-6Al-2Sn-4Zr-2Mo, (**c**) Ti-6Al-4V, and (**d**) Ti CP2.

Figure 6. PSD Voltage in H₂SO₄ (**a**) all samples, (**b**) Ti-6Al-2Sn-4Zr-2Mo, (**c**) Ti-6Al-4V, and (**d**) Ti CP2.

Table 4. Parameters obtained by PSD.

Ti-Alloys	B (dB (V))
NaCl	
Ti-6Al-2Sn-4Zr-2Mo	−20
Ti-6Al-4V	−11
Ti CP2	−8
H$_2$SO$_4$	
Ti-6Al-2Sn-4Zr-2Mo	−7
Ti-6Al-4V	−13
Ti CP2	−8

3.3. SEM Analysis

The corrosion product morphology micrographs of the titanium alloys and the elements present on the surface after SEM and EDS analyzed the electrochemical experiments; see Figures 7 and 8.
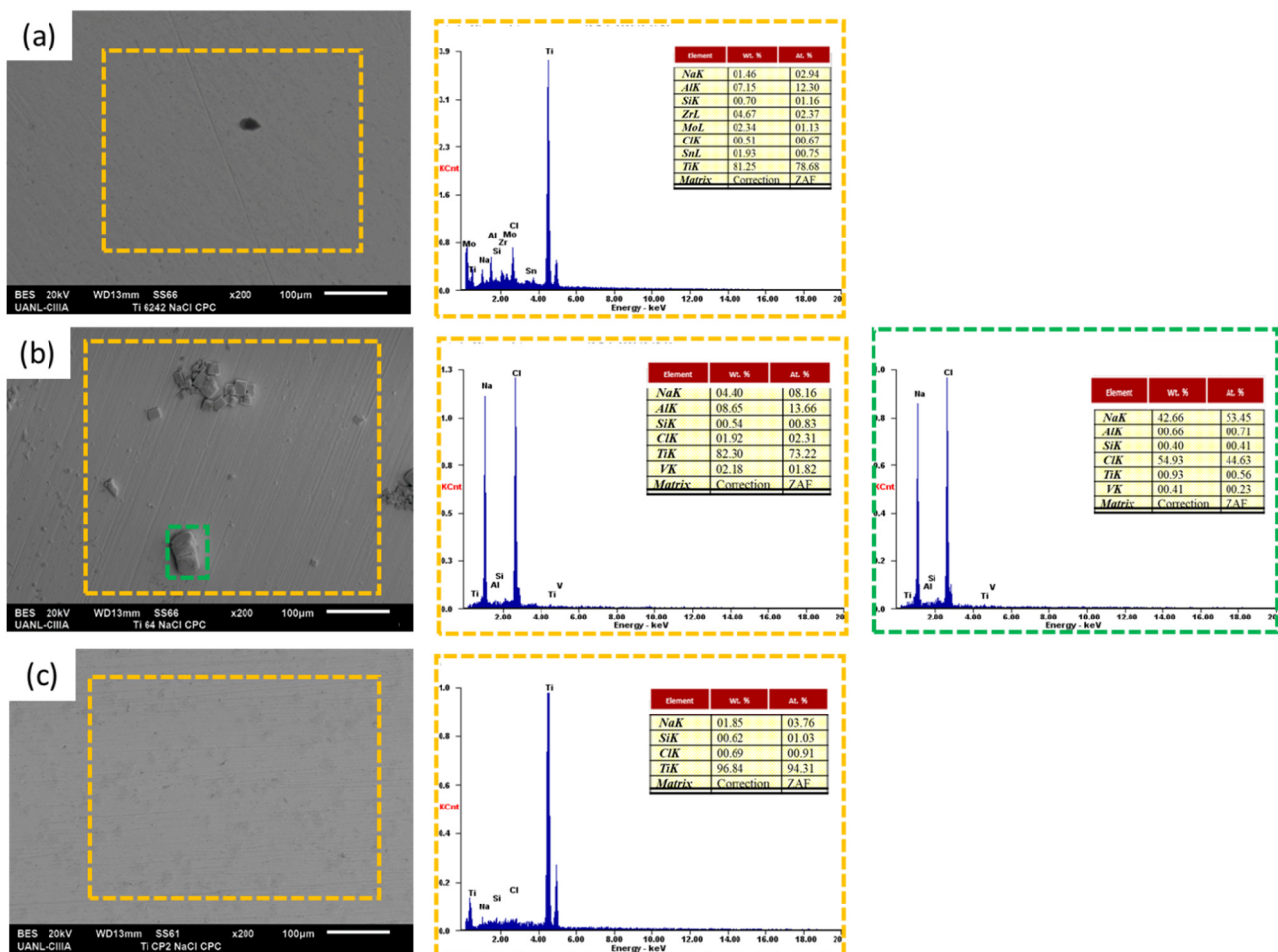
Figure 7. SEM-EDS surface morphology micrographs and EDS spectrum of titanium alloys exposed in a 3.5 wt % in NaCl solution, (**a**) Ti-6Al-2Sn-4Zr-2Mo, (**b**) Ti-6Al-4V, and (**c**) Ti CP2.
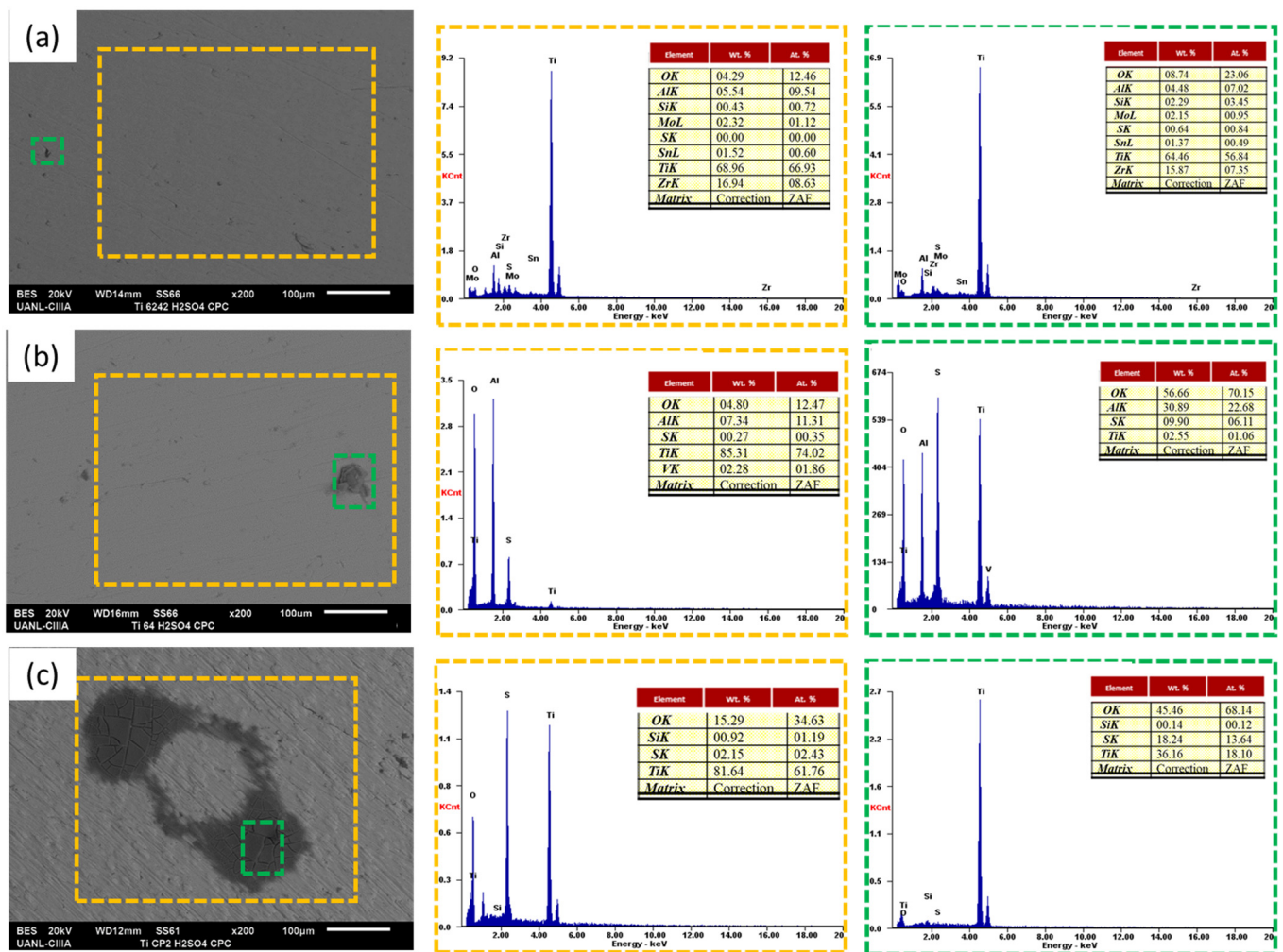
Figure 8. SEM-EDS surface morphology micrographs and EDS spectrum of titanium alloys exposed in a 3.5 wt % in H_2SO_4 solution, (**a**) Ti-6Al-2Sn-4Zr-2Mo, (**b**) Ti-6Al-4V, and (**c**) Ti CP2.

The presence of titanium, aluminum, zirconium, vanadium, molybdenum, and tin is observed in the EDS energy spectrum, corresponding to the base elements of the alloys under study.

In Figure 7a–c (EDS spectrum), Ti alloys in the NaCl solution did not have the presence of oxygen, but all (orange box) of them shows average Na (2.57 wt %) and Cl (1.04 wt %) on the surface, which indicates that the ions of Na^+ and Cl^- were diffused on the Ti-alloys surface. However, in Figure 7b (EDS spectrum, green box), a sodium chloride particle was observed on the surface of the Ti-6Al-4V alloy.

All samples present oxygen when Ti alloys are in H_2SO_4 solution (Figure 8a–c). However, it is more prevalent in Ti CP2, where oxygen in the darker zone, marked with an orange box (average 8.12 wt %), was higher than in the area marked with a green box (average 36.98 wt %). In addition, the spectra EDS of Figure 8 indicates that sulfur (average 9.59 wt %) was present. However, since the layer was not thick, surfaces did not significantly change color in areas.

4. Discussion

Titanium and its alloys depend on the chemical composition and alloying elements because they play a significant role in determining corrosion resistance [5,65]. In Froes et al. [66], the porosity of alloys compromises the mechanical strength and adequate pore size to obtain specific operating properties.

In Ti CP2 and Ti-6Al-4V samples, the microstructural analysis revealed the porosity, which causes loss of mechanical properties because pores are stress concentrators [65].

Seah et al. reported that although porosity makes material susceptible to localized corrosion, it can also repassivate. Therefore, an increase in the porosity of metals leads to a lower corrosion potential value, which results in increased susceptibility of porous materials to localized corrosion. It does assume that the relatively small pores present in the cell walls favor electrolyte placement and oxygen depletion, which is essential in the stability and preservation of the oxide layer on titanium. With open and interconnected pores, elements with higher porosity allow more effortless electrolyte flow, which complements the oxygen supply during the passivation process [67].

The higher values of E_{corr} are related to surface oxidation [68]. Dabrowski et al. [69] related that the porosity of titanium ranged from 45 to 75% with corrosion resistance. The material with higher porosity exhibited less corrosion susceptibility than those with 45% porosity. However, both elements exhibited lower corrosion resistance than the solid Ti [69]. Chen et al. confirmed that the electrolyte flow could also decrease solid and porous materials [70].

In this research, the porosity affected the generation of a homogenous passive layer. As pores are high-energy zones, current will accumulate in those areas generating reactions in anodic breach or pseudopassivation. Ti-6Al-2Sn-4Zr-2Mo was the alloy with higher porosity (2.88%). The NaCl electrolyte presents difficulties creating a homogenous passive layer; porosity is one factor that interferes with developing a continuous oxide layer. Even though pores affect the passive layer generation, it is essential to mention that all materials naturally present a porosity percentage linked with the manufacturing process. The pore diameters are in the order of 1–2 μm, minimizing influence in corrosion behavior.

Recent reports have shown resistance high corrosion resistance and difficulty of Cl^- ions to penetrate the metal surface. However, Cl^- can penetrate the oxide layer. Al-Saadi [36] determined that Cl^- ions penetrated surface film, creating adsorption of Cl^- in the oxide layer. According to values obtained in this research, Yang et al. [16] found 10^{-5} A·cm^2 for i_{corr}. Al-Saadi et al. also conclude that different types of localization do attribute to microstructure. The difference of phases causes localization problems for the passive layer. Yang mentioned that localization does accumulate on the β boundary. Nabhani et al. [64] associate the difference in oxide layer composition as a facilitator to Cl^- penetration because the oxide layer changes in the α and β phase. The α oxide layer is composed of a significant part of TiO_2 and is lesser in Al_2O_3 and the β oxide could be composed of vanadium or molybdenum. Both structures have higher pores because of atom distances and chloride ions penetrate those preferent zones as interstitial components. The difference in pores diameters avoids the generation of a stable passive layer notable in Ti-6Al-Sn-4Zr-2Mo. Pores bring forward a diffusion process [71–73], which reinforces Beck et al.'s research [74,75] on the susceptibility of Ti-alloys to halides. Perhaps Cl^- do not attack titanium surfaces at low potentials, but avoiding the homogenous passive layer developed. It can bring problems in prolongate time being sensitive to localized attacks, as De la Garza-Ramos et al. [76] conclude when Ti-6Al-4V do expose to the salt environment. Montoya Rangel et al. [77] conclude that when the protective layer did not present homogenous and continuous morphology, the corrosion protection will decrease, making materials susceptible to localized corrosion.

In the H_2SO_4 solution, all samples presented a passivation range, being the highest for Ti-6Al-2Sn-4Zr-2Mo, denoting a stable layer. Wang et al. [73] concluded that H_2SO_4 generates an oxide layer stable, but when halides are added in the solution layer developed pores, those halide concentrations increase according to critical values. Takahashi et al. [78] conclude that H_2SO_4 generates hydrolysis in the Ti4+ return in TiO_2 and is deposited on the surface. Cabral et al. [79,80] identify the generation of a stable passive layer with the capacity to restore itself with active–passive transition potential; for that reason, Ti-6Al-2Sn-4Zr-2Mo and Ti CP2 showed a stable behavior in H_2SO_4. Lara-Banda et al. [24,81] relate active potential with better passive layer stabilization. This phenomenon occurred for

Ti-6Al-2Sn-4Zr-2Mo that presented the E_{corr} most active of alloys and the highest passive range in H_2SO_4. According to Doll et al. [82], Ti-6Al-4V will form an oxide layer of TiO_2 with nanopores uniformly distributed at a long-time lapse of exposure. Although Ti-alloys developed a more stable passive layer in this research, corrosion rates are higher than in NaCl. This behavior could be attributed to the dissolution of the oxide layer and titanium surface covered by hydroxide or hydrated oxides [83,84]. In the return loop, an active anodic beach is observed, indicating the oxide layer dissolution. The same wet system can provoke surface humidity and facilitate layer dissolution.

For Ti-6Al-4V presented in an anodic breach, a phenomenon named by a diverse set of authors as a cathodic loop, Wang et al. [73] accredit this phenomenon to a change in electrolyte concentration, provoking oxide reduction and a change in pH solution. On the other hand, Lee et al. [85] related a cathodic loop with more parameters as a microstructure difference and scanning rates. However, they found that decreasing the scan rate E_{corr} trend to decrease. Besides, cathodic loops are present and related this phenomenon to a high OH^- concentration. Lee et al. [85] related a cathodic loop with oxygen discharge, so Ti-alloy increases the cathodic current; after that, Ti-alloy provides an oxidizing power to the system and generates a cathodic loop. In addition to Beavers [86] associated with oxygen or any oxidant agent in the test, Ramgopal et al. [87] and Cabral-Miramontes [88,89] obtained cathodic loops also and they associated it with protective layer reduction.

PSD results analyzed by the slope method showed results of uniform corrosion for Ti-6Al-2Sn-4Zr-2Mo. However, the other two Ti-alloys slope values are not in the corrosion type classified. This is in accordance with the conclusion of authors like Dawson, Uruchurtu, Homborg, Legat, and Lentka [90–93], where recommend do not use slope to determine the corrosion type. Uruchurtu, Dawson, and Legat recommend analyzing all the fluctuations in PSD; meanwhile, Homborg and Lenka suggest using other methods to analyze EN. This research corrosion type has collaborated with CPP, so slope values are associated with the passive and uniform process.

5. Conclusions

- Titanium alloys did not show susceptibility to pitting corrosion as observed in cyclic potentiodynamic polarization.
- The electrochemical results indicated that Ti-alloys developed passive layers in NaCl and H_2SO_4 solutions, but the passive layer is more stable in H_2SO_4 than the NaCl solution. Instability is related to Cl^- ions that avoids the proper layer growth.
- The passive layer was unstable for Ti-6Al-2Sn-4Zr-2Mo in the NaCl solution because Cl^- ions penetrated the oxide surface, being an unstable layer. CPP and PSD results confirm this with pseudopassivation and fluctuations, respectively. Further, molybdenum in the β phase facility the instability of the passive layer.
- Corrosion rates increase in the H_2SO_4 solution due to passive layer dissolution and the metal surface was exposed to the electrolyte.
- Ti-6Al-4V had higher corrosion rates; this did attribute to phases differences. β phase induced the development of vanadium oxide, which provoked an oxide layer with bigger pores so Cl^- and OH^- ions could penetrate the alloy. The difference in the oxide layer and OH^- concentration induced cathodic loops in Ti-6Al-4V.
- SEM observations presented diffusion of Cl^- and Na^+ on the material surface. For the H_2SO_4 solution, samples showed oxygen presence, but presence increase in Ti CP2, because this alloy did not have a phase difference, was only in α.
- Given the enormous industrial importance of this type of titanium alloy and by obtaining a better understanding of their corrosion behavior, we recognize that the use of powerful electrochemical techniques would be of great benefit.

References

1. Mouritz, P.A. *Introduction to Aerospace Materials*, 1st ed.; Woodhead Publishing: Cambridge, UK, 2012; pp. 202–223.
2. Gialanella, S.; Malandruccolo, A. *Aerospace Alloys*, 1st ed.; Springer: Cham, Switzerland, 2020; pp. 129–189.
3. Peters, M.; Hemptenmacher, J.; Kumpfert, J.; Leyens, C. *Structure and Properties of Titanium and Titanium Alloys*, 1st ed.; Wiley-VCH Verkag GmbG & Co. KGaA: Cologne, Germany, 2003; pp. 4–27.
4. Barington, N.; Black, M. Aerospace Materials and Manufacturing Processes at the Millennium. In *Aerospace Materials*; Cantor, B., Assender, H., Grant, P., Eds.; CRC Press: Boca Raton, FL, USA, 2002; pp. 3–15.
5. Jáquez-Muñoz, J.M.; Gaona-Tiburcio, C.; Cabral-Miramontes, J.; Nieves-Mendoza, D.; Maldonado-Bandala, E.; Olguín-Coca, J.; López-Léon, L.D.; Flores-De los Rios, J.P.; Almeraya-Calderón, F. Electrochemical Noise Analysis of the Corrosion of Titanium Alloys in NaCl and H_2SO_4 Solutions. *Metals* **2021**, *11*, 105. [CrossRef]
6. Koshal, D. Metal Casting and Moulding Processes. In *Manufacturing Engineer's Reference Book*; Koshal, D., Ed.; Butterworth Heinemann: Brighton, UK, 1993; pp. 1–23.
7. Yang, X.; Liu, C.R. Machining titanium and its alloys. *Mach. Learn.* **1998**, *3*, 107–139. [CrossRef]
8. Sha, W.; Malinov, S. *Titanium Alloys: Modelling of Microstructure, Properties and Applications*, 1st ed.; Malinov, S., Ed.; CRC Press: Oxford, UK, 2009; pp. 237–255.
9. Ahmad, Z. *Principles of Corrosion Engineering and Corrosion Control*, 1st ed.; Ahmad, Z., Ed.; Butterworth-Heinemann: London, UK, 2006; pp. 120–270.
10. Moiseyev, V.N. *Titanium Alloys Russian Aircraft and Aerospace Applications*, 1st ed.; Fridlayander, J.N., Eskin, D.G., Eds.; Taylor & Francis CRC Press: Boca Raton, FL, USA, 2005; pp. 164–173.
11. Klimecka-Tatar, D. Electrochemical characteristics of titanium for dental implants in case of the electroless surface modification. *Arch. Metall. Mater.* **2016**, *61*, 923–926. [CrossRef]
12. Klimecka-Tatar, D.; Borkowski, S.; Sygut, P. The kinetics of Ti-1Al-1Mn alloy thermal oxidation and characteristic of oxide layer. *Arch. Metall. Mater.* **2015**, *60*, 735–738. [CrossRef]
13. Jagielska-Wiaderek, K.; Bala, H.; Wierzchon, T. Corrosion depth profiles of nitrided titanium alloy in acidified sulphate solution. *Cent. Eur. J. Chem.* **2013**, *11*, 2005–2011. [CrossRef]
14. Liu, C.; Leyland, A.; Bi, Q.; Matthews, A. Corrosion resistance of multi-layered plasma-assisted physical vapour deposition TiN and CrN coatings. *Surf. Coat. Technol.* **2001**, *141*, 164–173. [CrossRef]
15. Balla, A.; Marcu, C.; Axante, D.; Borodi, G.; Lazar, D. Catalytic reduction of sulfuric acid to sulfur dioxide. *Cent. Eur. J. Chem.* **2012**, *10*, 1817–1823. [CrossRef]
16. Yang, X.; Dong, X.; Li, W.; Feng, W.; Xu, Y. Effect of solution and aging treatments on corrosion performance of laser solid formed Ti-6Al-4V alloy in a 3.5 wt. % NaCl solution. *J. Mater. Res. Technol.* **2020**, *9*, 1559–1568. [CrossRef]
17. Casillas, N.; Charlebois, S.; Smyrl, W.H.; White, H.S. Pitting Corrosion of Titanium. *J. Electrochem. Soc.* **1994**, *141*, 636. [CrossRef]
18. Du, X.; Yang, Q.S.; Chen, Y.; Zhang, X.Z. Galvanic Corrosion behavior of copper/titanium galvanic couple in artificial seawater. *Trans. Nonferrous Met. Soc. China* **2014**, *24*, 570–581. [CrossRef]
19. Fu, Y.; Zhou, F.; Wang, Q.; Zhang, M.; Zhou, Z. Electrochemical tribocorrosion performances of CrMoSiCN coating on Ti-6Al-4V titanium alloy in artificial seawater. *Corros. Sci.* **2020**, *165*, 108385. [CrossRef]
20. Caha, I.; Alves, A.C.; Chirico, C.; Tsipas, S.A.; Rodrigues, I.R.; Pinto, A.M.P.; Grandini, C.R.; Rocha, L.A.; Gordo, E.; Toptan, F. Interactions between wear and corrosion cast and sintered Ti-12Nb alloy in comparison with the commercial Ti-6Al-4V alloy. *Corros. Sci.* **2020**, *176*, 108925. [CrossRef]

21. Chen, W.Q.; Zhang, S.M.; Qiu, J. Surface analysis and corrosion behavior of pure titanium under fluoride exposure. *J. Prosthet. Dent.* **2020**, *124*, 239.e1–239.e8. [CrossRef]

22. Dubent, S.; Mazard, A. Characterization and corrosion behaviour of grade 2 titanium used in electrolyzers for hydrogen production. *Int. J. Hydrogen Energy* **2019**, *44*, 15622–15633. [CrossRef]

23. Lara-Banda, M.; Gaona-Tiburcio, C.; Zambrano-Robledo, P.; Delgado-E, M.; Cabral-Miramontes, J.A.; Nieves-Mendoza, D.; Maldonado-Bandala, E.; Estupiñan-López, F.; Chacón-Nava, J.G.; Almeraya-Calderón, F. Alternative to Nitric Acid Passivation of 15-5 and 17-4PH Stainless Steel Using Electrochemical Techniques. *Materials* **2020**, *13*, 2836. [CrossRef]

24. Nady, H.; El-Rabiei, M.M.; Samy, M. Corrosion behavior and electrochemical properties of carbon steel, commercial pure titanium copper and copper-aluminum-nickel alloy in 3.5% sodium chloride containing sulfide ions. *Egypt. J. Pet.* **2017**, *26*, 79–94. [CrossRef]

25. Magdy, A.M.; Ibrahim, D.; Yoshimura, P.M. The electrochemical behavior and characterization of the anodic oxide film formed on titanium in NaOH solutions. *J. Solid State Electrochem.* **2002**, *6*, 341–350. [CrossRef]

26. Lu, J.; Zhang, Y.; Huo, W.; Zhang, W.; Zhao, Y.; Zhang, Y. Electrochemical corrosion characteristics and biocompatibility of nanostructured titanium for implants. *Appl. Surf. Sci.* **2018**, *434*, 63–72. [CrossRef]

27. Hu, P.; Song, R.; Li, X.J.; Deng, J.; Chen, Z.Y.; Li, Q.W.; Wang, K.; Cao, W.; Liu, D.; Yu, H. Influence of concentrations of chloride ions on electrochemical corrosion behavior of titanium-zirconium-molybdenum alloy. *J. Alloys Compd.* **2017**, 367–372. [CrossRef]

28. Jelliti, S.; Richard, C.; Retraint, D.; Roland, T.; Chemkhi, M.; Demangel, C. Effect of surface nanocrystallization on the corrosion behavior of Ti-6Al-4V titanium alloy. *Sur. Coat. Technol.* **2013**, *224*, 82–87. [CrossRef]

29. Ji, R.; Wang, B.; Jin, H.; Liu, Y.; Cheng, W.; Cai, B.; Li, X. Removing loose oxide layer and producing dense α-phase layer simultaneously to improve corrosion resistance of Ti-6Al-4V titanium alloy by coupling electrical pulse and ultrasonic treatment. *Surf. Coat. Technol.* **2020**, *384*, 125329. [CrossRef]

30. Risking, J.; Khentov, A. *Electrocorrosion and Protection of Metals*, 2nd ed.; Risking, J., Ed.; Elsevier: Amsterdam, The Netherlands, 2019; pp. 225–248.

31. Kuphasuk, C.; Oshida, Y.; Andres, C.J.; Hovijitra, S.T.; Barco, M.T.; Brown, D.T. Electrochemical corrosion of titanium and titanium-based alloys. *J. Prothet. Dent.* **2001**, *85*, 195–202. [CrossRef]

32. Pink, H.; Rui, S.; Kuaishe, W.; Fan, Y.; Boliang, H.; Zhen-Lu, C.; Qinwe, L.; Weicheng, C.; Dongxin, L.; Lei, G.; et al. Electrochemical Corrosion Behavior of Titanium-Zirconium-Molybdenum Alloy. *Rare Metal Mat. Eng.* **2017**, *46*, 1225–1230. [CrossRef]

33. Tang, X.; Ahmed, T.; Rack, H.J. Phase transformations in Ti-Nb-Ta and Ti-Nb-Ta-Zr alloys. *J. Mater. Sci.* **2000**, *35*, 1805–1811. [CrossRef]

34. Soltis, J. Passivity breakdown, pit initiation and propagation of pits in metallic materials—Review. *Corr. Sci.* **2015**, *90*, 5–22. [CrossRef]

35. Natishan, P.M.; O'Grady, W.R. Chloride Ion Interactions with Oxide-Covered Aluminum Leading to Pitting Corrosion: A Review. *J. Electrochem. Soc.* **2014**, *161*, C421–C432. [CrossRef]

36. Al-Saadi, S.; Yi, Y.; Cho, P.; Jang, C.; Beeley, P. Passivity breakdown of 316L stainless steel during potentiodynamic polarization in NaCl solution. *Corros. Sci.* **2016**, 720–727. [CrossRef]

37. Seo, D.; Lee, J.B. Effects of competitive anion adsorption (Br- or Cl-) and semiconducting properties of the passive films on the corrosion behavior of the additively manufactured Ti-6Al-4V alloys. *Corros. Sci.* **2020**, *173*, 108789. [CrossRef]

38. Galván-Martinez, R.; Orozco-Cruz, R.; Torres-Sanchez, R.; Martinez, E.A. Corrosion study of the X52 steel immersed in seawater with a corrosion inhibitor using a rotating cylinder electrode. *Mater. Corros.* **2010**, *61*, 872–876. [CrossRef]

39. Corral-Higuera, R.; Arredondo-Rea, P.; Neri-Flores, M.A.; Gómez-Soberón, J.M.; Almaral-Sánchez, J.L.; Castorena-González, J.C.; Almeraya-Calderón, F. Chloride ion penetrability and Corrosion Behavior of Steel in Concrete with Sustainability Characteristics. *Int. J. Electrochem. Sci.* **2011**, *6*, 958–970.

40. Noel, J.J.; Shoesmith, D.W. *Ebrahimi, N. Corrosion of Titanium, and Its Alloys*, 1st ed.; Wandelt, K., Ed.; Elsevier: Amsterdam, The Netherlands, 2016; pp. 193–199.

41. Galván-Martínez, R.; Cabrera-de la Cruz, D.; Contreras, A.; Orozco-Cruz, R. A novel experimental arrangement for corrosión study of X60 pipeline steel weldments at turbulent flow conditions. *Corros. Eng. Sci. Technol.* **2016**, *5*, 1–8. [CrossRef]

42. Gaona-Tiburcio, C.; Aguilar, L.M.R.; Zambrano-Robledo, P.; Estupiñán-López, F.; Cabral-Miramontes, J.A.; Nieves-Mendoza, D.; Castillo-González, E.; Almeraya-Calderón, F. Electrochemical Noise Analysis of Nickel Based Superalloys in Acid Solutions. *Int. J. Electrochem. Sci.* **2014**, *9*, 523–533.

43. Estupiñán-López, H.F.; Almeraya-Calderón, F.; Bautista Margulis, G.R.; Baltazar Zamora, M.A.; Martínez-Villafañe, A.; Uruchurtu, C.J.; Gaona-Tiburcio, C. Transient Analysis of Electrochemical Noise for 316 and Duplex 2205 Stainless Steels Under Pitting Corrosion. *Int. J. Electrochem. Sci.* **2011**, *6*, 1785–1796.

44. Contreras, A.; Salazar, M.; Carmona, A.; Galván-Martínez, R. Electrochemical Noise for Detection of Stress Corrosion Cracking of Low Carbon Steel Exposed to Synthetic Soil Solution. *Mater. Res.* **2017**, *20*, 1–10. [CrossRef]

45. Sedriks, A.J.; Green, J.A.; Novak, D.L. Electrochemical behavior of Ti-Ni alloys in acidic chloride solutions. *Corrosion* **1972**, *28*, 137–142. [CrossRef]

46. Tafel, J. Über die polarization bei kathodischer wasserstoffentwicklung. *Z. Phys. Chem.* **1905**, 641–712. [CrossRef]

47. Wagner, C.; Traud, W. *Über die Deutung von Korrosionsvorgängen durch Überlagerung von elektrochemischen Teilvorgängen und über die Potentialbildung an Mischelektroden, Z. Elektrochem*; Springer: Berlin/Heidelberg, Germany, 1951; pp. 391–454. [CrossRef]

48. Butler, J.A.V. Studies in heterogeneous equilibria. Part II.—The kinetic interpretation on the Nernst theory of electromotive force. *Trans. Faraday Soc.* **1924**, 729–733. [CrossRef]

49. Erdey-Gruz, T.; Volmer, M. Zur Theorie der Wasserstoff Überspannung. *Z. Phys. Chem.* **1930**, *150*, 203–213. [CrossRef]

50. Esmailzadeh, S.; Aliofkhazraei, M.; Sarlak, H. Interpretation of Cyclic Potentiodynamic Polarization Test Results for Study of Corrosion Behavior of Metals: A Review. *Prot. Met. Phys. Chem. Sulf.* **2018**, *54*, 976–989. [CrossRef]

51. Silverman, D.C. *Tutorial on Cyclic Potentiodynamic Polarization Technique*; NACE Corrosion/98; NACE International: Houston, TX, USA, 1998.

52. McCafferty, E. Validation of corrosion rates measured by the Tafel extrapolation method. *Corros. Sci.* **2005**, *47*, 3202–3215. [CrossRef]

53. Beck, T.R.; Blackburn, M.J.; Smyrl, W.H. Stress Corrosion Cracking of Titanium Alloys: Electrochemical kinetics, SCC Studies with Ti:8-1-1, SCC and Polarization Curves in Molten Salts, Liquid Metal Embrittlement, and SCC Studies with other Titanium Alloys. In *Solid State Physics Laboratory*; Boeing Scientific Research Laboratories: Seattle, WA, USA, 1969.

54. Cabral-Miramontes, J.A.; Gaona-Tiburcio, C.; Almeraya-Calderón, F.; Estupiñan-Lopez, H.F.; Pedraza-Basulto, G.; Poblano-Salas, C. Parameter Studies on High-Velocity Oxy-Fuel Spraying of CoNiCrAlY Coatings Used in the Aeronautical Industry. *Int. J. Corros.* **2014**, 1–8. [CrossRef]

55. Kearns, J.R.; Eden, D.A.; Yaffe, M.R.; Fahey, J.V.; Reichert, D.L.; Silverman, D.C. *ASTM Standardization of Electrochemical Noise Measurement. Electrochemical Noise Measurement for Corrosion Applications*; Kearns, J.R., Scully, J.R., Roberge, P.R., Reirchert, D.L., Dawson, L., Eds.; ASTM International, Materials Park: Novelty, OH, USA, 1996; pp. 446–471.

56. Botana, P.J.; Bárcena, M.M.; Villero, Á.A. *Ruido Electroquímico: Métodos de Análisis*; Septem Ediciones: Cadiz, Spain, 2002; pp. 50–70.

57. Legat, A.; Dolecek, V. Corrosion Monitoring System Based on Measurement and Analysis of electrochemical Noise. *Corrosion* **1995**, *51*, 295–300. [CrossRef]

58. Ohtsuka, T.; Nishikata, A.; Sakairi, M.; Fushimi, K. *Electrochemistry for Corrosion Fundamentals*; Springer Singapore: Singapore, 2018; pp. 140–156.

59. ASTM E3-95. *Standard Practice for Preparation of Metallographic Specimens*; ASTM International: West Conshohocken, PA, USA, 1995.

60. ASTM E407-07. *Standard Practice for Microetching Metals and Alloys*; ASTM International: West Conshohocken, PA, USA, 2011.

61. ASTM G5—14e1. *Standard Reference Test Method for Making Potentiodynamic Anodic Polarization Measurements*; ASTM International: West Conshohocken, PA, USA, 2014.

62. ASTM G61-86. *Standard Test Method for Conducting Cyclic Potentiodynamic Polarization Measurements for Localized Corrosion Susceptibility of Iron, Nickel or Cobalt-Based Alloys*; ASTM International: West Conshohocken, PA, USA, 1998.

63. ASTM G199-09. *Standard Guide for Electrochemical Noise Measurement*; ASTM International: West Conshohocken, PA, USA, 2009.

64. Nabhani, M.; Razavi, R.S.; Barekat, M. Corrosion study of laser cladded Ti-6Al-4V alloy in different corrosive environments. *Eng. Fail. Anal.* **2019**, *97*, 234–241. [CrossRef]

65. Bocchetta, P.; Chen, L.-Y.; Tardelli, J.D.C.; Reis, A.C.d.; Almeraya-Calderón, F.; Leo, P. Passive Layers and Corrosion Resistance of Biomedical Ti-6Al-4V and β-Ti Alloys. *Coatings* **2021**, *11*, 487. [CrossRef]

66. Froes, F.; Quian, M. *Titanium for Consumer Applications. Real World Use of Titanium*; Elsevier Inc.: Amsterdam, The Netherlands, 2019; pp. 27–65. [CrossRef]

67. Seah, K.H.W.; Thampuran, R.; Teoh, S.H. The influence of pore morphology on corrosion. *Corros. Sci.* **1998**, *40*, 547–556. [CrossRef]

68. Adamek, G.; Pałka, K.; Jakubowicz, J. Corrosion properties of Ti scaffolds prepared with sucrose as a space holder. *Solid State Phenom.* **2015**, *227*, 519–522. [CrossRef]

69. Dabrowski, B.; Kaminski, J.; Swieszkowski, W.; Kurzydlowski, K.J. Porous titanium scaffolds for biomedical applications: Corrosion resistance and structure investigation. *Mater. Sci. Forum* **2011**, *674*, 41–46. [CrossRef]

70. Chen, X.; Fu, Q.; Jin, Y.; Li, M.; Yang, R.; Cui, X.; Gong, M. In vitro studying corrosion behavior of porous titanium coating in dynamic electrolyte. *Mater. Sci. Eng. C* **2017**, *70*, 1071–1075. [CrossRef]

71. Prando, D.; Nicolis, D.; Pedeferri, M.; Ormellese, M. Pitting corrosion on anodized titanium: Effect of halades. *Mater. Corros.* **2018**, *69*, 1–6. [CrossRef]

72. Maldonado-Bandala, E.; Jiménez-Quero, V.; Olguin-Coca, J.; Lizarraga, L.G.; Baltazar-Zamora, M.A.; Ortiz-C, A.; Almeraya, C.F.; Zambrano, R.P.; Gaona-Tiburcio, C. Electrochemical Characterization of Modified Concretes with Sugar Cane Bagasse Ash. *Int. J. Electrochem. Sci.* **2011**, *6*, 4915–4926.

73. Wang, Z.B.; Hu, H.X.; Zheng, Y.G. Synergistic effects of fluoride and chloride on general corrosion behavior of AISI 316 stainless steel and pure titanium in H2SO4 solutions. *Corros. Sci.* **2018**, *130*, 203–217. [CrossRef]

74. Beck, T.R.; Blackburn, M.J. Stress corrosion cracking of titanium alloys. *AIAA J.* **1968**, *6*, 326–332. [CrossRef]

75. Gao, K.W.; Chu, W.Y.; Gu, B.; Zhang, T.C.; Qiao, L.J. In-Situ Transmission Electron Microscopic Observation of Corrosion-Enhanced Dislocation Emission and Crack Initiation of Stress Corrosion. *Corrosion* **2000**, *56*, 515–522. [CrossRef]

76. De la Garza-Ramos, M.A.; Estupiñan-Lopez, F.H.; Gaona-Tiburcio, C.; Beltrán-Novelo, L.G.; Zambrano-Robledo, P.; Cabral-Miramontes, J.; Almeraya-Calderón, F. Electrochemical Behavior of Ti6Al4V Alloy Used in Dental Implants Immersed in Streptococcus gordonii and Fusobacterium nucleatum Solutions. *Materials* **2020**, *13*, 4185. [CrossRef]

77. Almeraya-Calderón, F.; Montoya-R, M.; Garza Montes de Oca, N.; Castorena, J.H.; Estupiñan, F.; Cabral, J.; Maldonado, E.; Gaona-Tiburcio, C. Corrosion behavior of multilayer Coatings deposited by PVD Inconel 718 in Chloride and Sulphuric Acid solutions. *Int. J. Electrochem. Sci.* **2019**, *14*, 9596–9609. [CrossRef]

78. Takahashi, K.; Kagawa, T.; Tanaka, K.; Kihira, H.; Ushioda, K. Reduction of Contact Resistance on Titanium Sheet Surfaces by Formation of Titanium Carbide and Nitride, and its Stability in Sulfuric Acid Aqueous Solution. *ISIJ Int.* **2019**, *59*, 1621–1631. [CrossRef]

79. Cabral-Miramontes, J.; Gaona-Tiburcio, C.; Estupinán-López, F.; Lara-Banda, M.; Zambrano-Robledo, P.; Nieves-Mendoza, D.; Maldonado-Bandala, E.; Chacón-Nava, J.; Almeraya-Calderón, F. Corrosion Resistance of Hard Coat Anodized AA 6061 in Citric–Sulfuric Solutions. *Coatings* **2020**, *10*, 601. [CrossRef]

80. Cabral-Miramontes, J.A.; Barceinas-Sánchez, J.D.O.; Poblano-Salas, C.A.; Pedraza-Basulto, G.K.; Nieves-Mendoza, D.; Zambrano-Robledo, P.C.; Almeraya-Calderón, F.; Chacón-Nava, J.G. Corrosion Behavior of AISI 409Nb Stainless Steel Manufactured by Powder Metallurgy Exposed in H_2SO_4 and NaCl Solutions. *Int. J. Electrochem. Sci.* **2013**, *8*, 564–577.

81. Pellegrini-Cervantes, M.J.; Almeraya-Calderon, F.; Borunda-Terrazas, A.; Bautista-Margulis, R.G.; Chacón-Nava, J.G.; Fajardo-San-Miguel, G.; Almaral-Sanchez, J.L.; Barrios-Durstewitz, C.; Martinez-Villafañe, A. Corrosion Resistance, Porosity and Strength of lended Portland Cement Mortar Containing Rice Husk Ash And Nano-SiO$_2$. *Int. J. Electrochem. Sci.* **2013**, *8*, 10697–10710.

82. Doll, P.W.; Wolf, M.; Weichert, M.; Ahrens, R.; Spindler, B.; Guber, A.E. Nanostructuring of Titanium by Anodic Oxidation with Sulfuric and Hydrofluoric Acid. *Curr. Direc. Biomed. Eng.* **2018**, *4*, 641–644. [CrossRef]

83. Krýsa, J.; Mráz, R.; Sousar, I. Corrosion rate of titanium in H_2SO_4. *Mat. Chem. Phys.* **1997**, *48*, 64–67. [CrossRef]

84. Zhao, Y.; Zhou, E.; Xu, D.; Yang, Y.; Zhao, Y.; Zhang, Y.; Gu, T.; Yang, K.; Wang, F. Laboratory investigation of microbiologically influenced corrosion of 2205 duplex stainless steel by marine pseudomonas aeruginosa biofilm using electrochemical noise. *Corrosion* **2018**, *143*, 291. [CrossRef]

85. Lee, J.W.; Osseo-Asare, K.; Pickering, H.W. Anodic dissolution of iron in ammoniacal ammonium carbonate solution. *J. Electrochem. Soc.* **1985**, *132*, 550. [CrossRef]

86. Beavers, J.A.; Durr, C.L.; Thompson, N.G. Unique Interpretations of Potentiodynamic Polarization Technique. In *NACE International: Corrosion/98, San Diego, California*; paper 300; 1998.

87. Ramgoal, T.; Schmutz, P.; Frankel, G.S. Electrochemical Behavior of Thin Film Analogs of Mg (Zn, Cu, Al)2. *J. Electrochem. Soc.* **2001**, *148*, B348. [CrossRef]

88. Cabral-Miramontes, J.A.; Bastidas, D.M.; Baltazar, M.A.; Zambrano-Robledo, P.; Bastidas, J.M.; Almeraya-Calderón, F.M.; Gaona-Tiburcio, C. Corrosion behavior of Zn-TiO$_2$, and Zn-ZnO Electrodeposited Coating in 3.5% NaCl Solution. *Int. J. Electrochem. Sci.* **2019**, *14*, 4226–4239. [CrossRef]

89. Cabral Miramontes, J.A.; Barceinas Sánchez, J.D.O.; Almeraya Calderón, F.; Martínez Villafañe, A.; Chacón Nava, J.G. Effect of Boron Additions on Sintering and Densification of a Ferritic Stainless Steel. *J. Mater. Eng. Perform.* **2010**, *19*, 880–884. [CrossRef]

90. Hernández, M.; Genescá, J.; Uruchurtu, J.; Barba, A. Correlation between electrochemical impedance and noise measurements of waterborne coatings. *Corr. Sci.* **2009**, 499–510. [CrossRef]

91. Uruchurtu, J.C.; Dawson, J.L. Noise Analysis of Pure Aluminum under Different Pitting Conditions. *Corrosion* **1987**, *43*, 19–26. [CrossRef]

92. Lentka, L.; Smulko, J. Methods of trend removal in electrochemical noise data-overview. *Measurement* **2019**, *131*, 569–581. [CrossRef]

93. Homborg, A.M.; Cottis, R.A.; Mol, J.M.C. An integrated approach in the time, frequency and time-frequency domain for the identification of corrosion using electrochemical noise. *Electrochim. Acta* **2016**, *222*, 627–640. [CrossRef]